Neutron Emission and Fission Energetics in the Proton-Induced Fission of ^{233}U and ^{238}U†

S. C. Burnett,* R. L. Ferguson, F. Plasil, and H. W. Schmitt

Oak Ridge National Laboratory, Oak Ridge, Tennessee 37830
(Received 28 December 1970)

Energetics of the fission of ^{233}U induced by 8.5- and 13-MeV protons and of ^{238}U induced by 12-MeV protons have been studied by means of a three-parameter experiment in which the time of flight of one fragment and the energies of both fragments are measured. The average number of neutrons emitted from the individual fragments and from both fragments together are obtained as functions of fragment mass and total kinetic energy. The number of neutrons emitted per fragment generally increases with increasing fragment mass, and the "sawtooth" shape characteristic of neutron emission in low-excitation fission is still apparent, although the relative depths of the minimum in each of the present cases is reduced. A comparison of the number of neutrons emitted as a function of fragment mass for 8.5- and 13-MeV proton-induced fission of ^{233}U shows that excitation energies of the light fragments change only slightly, while those of the heavy fragments increase significantly with increasing bombarding energy. The largest change occurs in the mass region at about 132 amu, where the doubly-closed-shell configuration $Z=50$, $N=82$ occurs. Pre- and post-neutron-emmission fragment mass distributions are obtained, together with the fragment energy distributions and mass-versus-energy correlations. Energy balance is studied by comparing the total energy available for fission into a given mass pair with the sum of the fragment excitation energies, calculated from neutron emission data and mass tables, and the measured fragment kinetic energies. The results are discussed within the framework of simple theoretical fission models.

I. INTRODUCTION

The experiment reported in this paper was designed specifically to establish the relationship between ΔE^*_{CN}, an increment in the excitation energy of a fissioning compound nucleus, and the resulting increments in prompt total fragment kinetic energy (ΔE^*_K) and in the prompt individual fragment excitation energies (ΔE_{XL} and ΔE_{XH}). For this purpose the $^{233}U(p,f)$ reaction was studied at proton bombarding energies of 8.5 and 13.0 MeV. In addition, a measurement was made for the $^{238}U(p,f)$ reaction at $E_p = 12.0$ MeV.

The number of neutrons emitted per fragment, from which the fragment excitation energy is inferred, was obtained as a function of fragment mass; detailed fragment mass and energy probability distributions and correlations were also obtained. The results provide a basis for further understanding of the fission process, in particular that portion of the process during which fragment formation and scission occur.

Neutron emission measurements with simultaneous determination of fragment masses and kinetic energies have been made for fission at low excitation energies.[1-4] Such data for a few cases of medium excitation fission have become available only within the past few years: these include measurements on $^{226}Ra(p,f)$,[5] $^{238}U(p,f)$,[6] and $^{209}Bi(\alpha,f)$.[7] Preliminary results of the present experiment on $^{233}U(p,f)$ were reported earlier,[8] and an experiment showing similar trends was reported recently by Bishop *et al.*[9]

To avoid background and detection-efficiency problems inherent in neutron counting experiments, we have made use of an indirect method for determining neutron emission,[10] which has been shown to give results for ^{252}Cf in agreement with those of direct neutron counting experiments. The method, based on the simultaneous measurement of the kinetic energies of both fragments and the velocity of one of them, has been used in $^{226}Ra(p,f)$[5] and $^{209}Bi(\alpha,f)$[7] experiments at this laboratory; a variation of the method was used by Derengowski and Melkonian[4] in $^{235}U(n_{thermal},f)$ experiments. A brief description of the method used in this work is given in Sec. II.

The uncertainty of the method in determining $\nu(m^*)$, the average number of neutrons emitted as a function of prompt fragment mass, is about ±0.5 neutron on an absolute scale. In this work, however, we have made careful comparison measurements at two compound-nucleus excitation energies; the uncertainty in the difference of $\nu(m^*)$ values at the two energies is therefore only about ±0.2 neutron.

Targets of ^{233}U were bombarded with 8.5- and 13.0-MeV protons, and a target of ^{238}U with 12-MeV protons. The choice of the first two energies was determined by the upper energy limit

of the Oak Ridge tandem Van de Graaff on the one hand, and by the rapid decrease of cross section with decreasing proton energy (Coulomb-barrier penetrability) on the other. The choice of the $^{233}U(p,f)$ reaction was made because, over the above energy range, the probability for second-chance fission was estimated to be essentially constant and smaller than that for other available targets. Thus any differences observed in the comparison study should be the result of differences in compound-nucleus excitation energy and not of differences in the compound nucleus. The choice of the 12-MeV proton bombardment of ^{238}U was made so that the results of the present method of measurement could be compared directly with those of a direct neutron counting experiment of Cheifetz and Fraenkel.[6] Absolute calibration experiments with ^{252}Cf were carried out as discussed in Ref. 10.

Results for each case include arrays showing the number of events as a function of fragment mass and total kinetic energy, and the average number of neutrons emitted from single fragments and from both fragments together as functions of fragment mass and total kinetic energy. A number of correlations and distributions can be obtained from these arrays and a systematic presentation of results is given in Sec. III. Section IV gives a brief discussion of total energy balance. Section V includes discussion of the comparison of the 8.5- and 13.0-MeV results for $^{233}U(p,f)$. Some ideas regarding interpretation of the data are included.

II. EXPERIMENT

Summarized in Table I are the characteristics of the proton beam and fissile targets, geometric parameters, including source and detector sizes and source-to-detector distances, and the number of events accumulated in each of the runs which make up this experimental study. The $^{233}U(p,f)$ experiments are denoted (a), (b), (c), and (d) and were carried out at proton energies of 13.0, 8.5, 8.5, and 13.0 MeV, respectively. Experimental parameters for the $^{238}U(p,f)$ experiment, for which the proton energy was 12.0 MeV, and for the ^{252}Cf calibration experiments are also included in Table I.

The experimental arrangement, including electronics, was similar to that shown schematically in Ref. 5. The aluminum vacuum chamber was equipped with antiscattering baffles along the fission-fragment flight path to prevent the detection of fission fragments scattered from the walls of the flight tube. A silicone oil diffusion pump, equipped with water-cooled baffles, provided a vacuum of 10^{-6} Torr.

Proton beams were obtained from the Oak Ridge tandem Van de Graaff accelerator. The chamber was equipped with moveable, externally controlled quartz cross hairs that could be accurately positioned and viewed while the beam was on and the system under vacuum. This optical reference point, along with precise proton-beam collimation, made possible accurate determination of the beam and target positions with respect to detector positions. The sizes and positions of the fragment detectors and the distances of the detectors from the fissioning source, tabulated in Table I, were such that for every fragment incident on the remote detector, the complementary fragment was incident on the near detector.

The ^{252}Cf source (10^5 fissions/min) was made by self-transfer onto a 5-μin.-thick nickel backing. The uranium targets were prepared by vacuum evaporation onto thin carbon films. Thick-

TABLE I. Summary of experimental conditions.

		Detector Pair 1					Detector Pair 2	
	Target (or ^{252}Cf source)	^{238}U	^{233}U	^{233}U	^{233}U	^{252}Cf	^{233}U	^{252}Cf
	^{233}U experiment label		(a)	(b)	(c)		(d)	
	Deposit thickness ($\mu g/cm^2$)	≈50	≈190	≈190	≈60	0	≈60	0
	Fragment energy loss in deposit (MeV)	≈0.8	≈3.1	≈3.1	≈1.0	0	≈1.0	0
	Fragment energy loss in backing (MeV)	≈1.6	≈3.3	≈3.3	≈2.6	≈4.0	≈2.6	≈4.0
	Proton bombarding energy (MeV)	12.0	13.0	8.5	8.5	•••	13.0	•••
	Beam current (nA)	100	100	110	110	•••	100	•••
	Beam size (cm^2)	0.18	0.32	0.32	0.32	•••	0.32	•••
Detector 1	Active area (cm^2)	5.0	5.0	5.0	5.0	5.0	2.0	2.0
Detector 1	Distance to source, A (cm)	105.24	105.24	105.24	105.24	105.37	105.24	105.37
Detector 2	Active area (cm^2)	3.0	3.0	3.0	3.0	3.0	3.0	3.0
Detector 2	Distance to source, B (cm)	5.78	5.76	5.76	5.76	5.63	5.76	5.63
	Number of events	57 938	51 184	21 326	8714	56 649	51 193	57 347

nesses of deposits and backings are tabulated in Table I.

In the calibration experiments the ^{252}Cf source was oriented parallel to and coaxially with the detector surfaces, with the deposit facing the remote detector. In the uranium experiments the targets were oriented at 45° with respect to both the beam axis and the detector surfaces, with the deposits facing the incoming beam and the remote detector.

Analysis of the correlated event-by-event data, accumulated in 256 channels in each parameter, was carried out with the aid of a digital computer.

Three quantities have been measured for each event: two pulse-heights related to the kinetic energies E_1 and E_2 of the two fragments and the time of flight of one fragment from which its velocity, v_1, was obtained. The post-neutron emission mass, m_1, of fragment number one was calculated directly from the relationship $m_1 = 2E_1/v_1^2$. The preneutron-emission mass of fragment 1 is given from momentum conservation by

$$m_1^* = A_{CN}/(1 + v_1^*/v_2^*),$$

where A_{CN} is the mass of the compound nucleus and the asterisks refer to quantities before neutron emission. It can be shown that m_1^* can be approximated by

$$m_1^* = A_{CN}/[1 + (E_1 m_2/E_2 m_1)^{1/2}].$$

In this expression all quantities are known with the exception of m_2, the post-neutron-emission mass of the fragment impinging on the near detector. In place of a particular m_2 value for every given specific event, an average value $\bar{m}_2$ was used for every particular combination of energies E_1 and E_2. These averages were evaluated from the m_1 data, and the principle of symmetry was applied for the purpose of obtaining $\bar{m}_2$ values. This method of complementary points is discussed fully in Ref. 10, which includes a description of the complete method of data analysis. The number of neutrons ν_1 emitted from fragment 1 was finally calculated for each event from the relationship

$$\nu_1 = m_1^* - m_1.$$

Appendix I contains further discussion of the details of the various runs as they relate to data analysis and determination of the final results. Possible sources of error or uncertainty in the experiment are evaluated and discussed in Appendix II; a discussion of the effect of prefission neutron emission on the results is included.

III. RESULTS

The results of a three-parameter experiment of this kind may in principle be shown in a variety

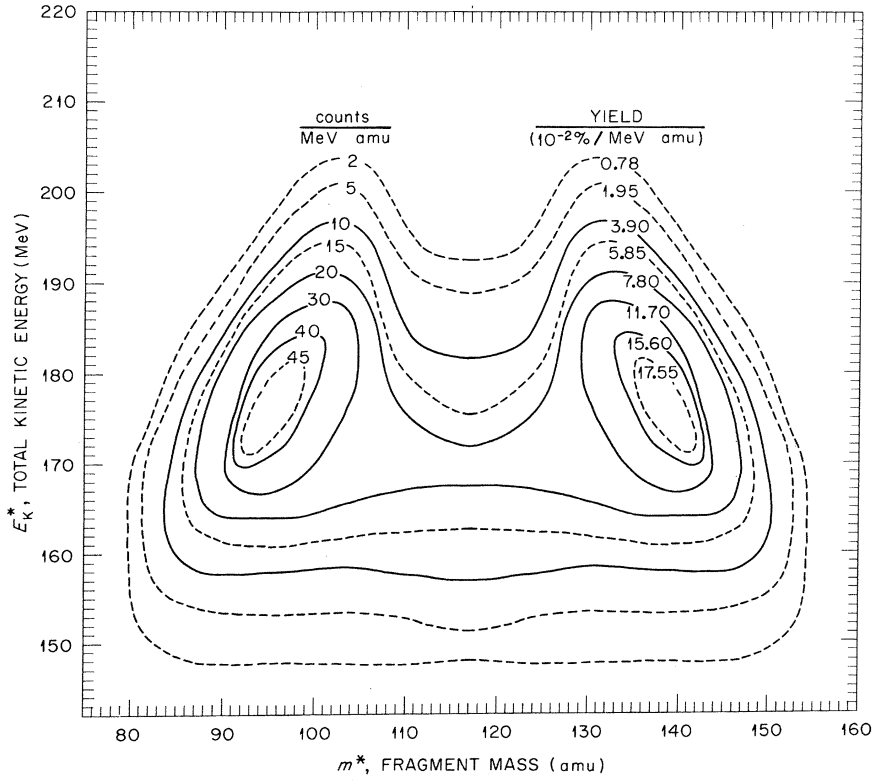

FIG. 1. Contour diagram of fission yields as a function of prompt fragment mass and total kinetic energy of both fragments for ^{233}U(p,f), $E_p = 13$ MeV.

of ways, with the numerous available variables taken singly or in combination. Here we shall show and discuss the results primarily in terms of the following quantities: pre-neutron-emission fragment mass m^*, total pre-neutron-emission kinetic energy E_K^* of fragment pairs,[11] and number of neutrons emitted ν (for single fragments) and ν_T (for fragment pairs). Yield is designated by N (number of counts) or Y (fractional yield). Results are presented for the three fissioning systems investigated: ^{233}U bombarded by 8.5- and 13.0-MeV protons, referred to as $^{233}U(p_{8.5},f)$ and $^{233}U(p_{13},f)$, respectively, and ^{238}U bombarded by 12.0-MeV protons, $^{238}U(p_{12},f)$.

A. Fragment Masses and Kinetic Energies

The contour diagrams of Figs. 1–3 show the fragment mass vs total kinetic energy correlations $N(m^*, E_K^*)$. Asymmetric mass divisions predominate in all cases, but appreciable yields from symmetric and near symmetric divisions are also present over a broad range of kinetic energies. We have taken advantage of the symmetric nature of these arrays to average complementary points left and right of symmetry, thereby improving somewhat the statistical accuracy of the contours. They are thus rendered exactly symmetric in the figures, small statistical differences having been reduced by this process. Fragment yields are normalized to 200% total yield.

It may be seen in the figures that the most probable mass divisions tend toward splits yielding heavy fragments with $m^* \cong 132$ amu when the total fragment kinetic energy approaches its maximum value, as has also been noted frequently in the literature for low-excitation fission.

In Figs. 4–6, for $^{233}U(p_{13},f)$, $^{233}U(p_{8.5},f)$, and $^{238}U(p_{12},f)$, respectively, we show fragment yields summed over all kinetic energies, average total kinetic energies $\langle E_K^* \rangle$, and the rms widths $\sigma_{E_K^*}$ of the total kinetic energy distributions as functions of prompt fragment mass. Also plotted in the lower sections of these figures are the mass yield distributions of post-neutron-emission fragments; these are shifted to slightly lower masses with respect to the pre-neutron-emission distributions.

Peak-to-valley ratios of the prompt mass yield distributions are 2.2 for $^{233}U(p_{13},f)$, 6.8 for $^{233}U(p_{8.5},f)$, and 6.1 for $^{238}U(p_{12},f)$.

Peaks in the $\langle E_K^* \rangle$ vs m^* curves correspond, for all three systems, to a heavy fragment mass ~132 amu. The dip in kinetic energy at symmetric mass divisions is 9 MeV for $^{233}U(p_{13},f)$, 12 MeV for $^{233}U(p_{8.5},f)$, and 13 MeV for $^{238}U(p_{12},f)$. The $\sigma_{E_K^*}$ curves are similar for all three systems,

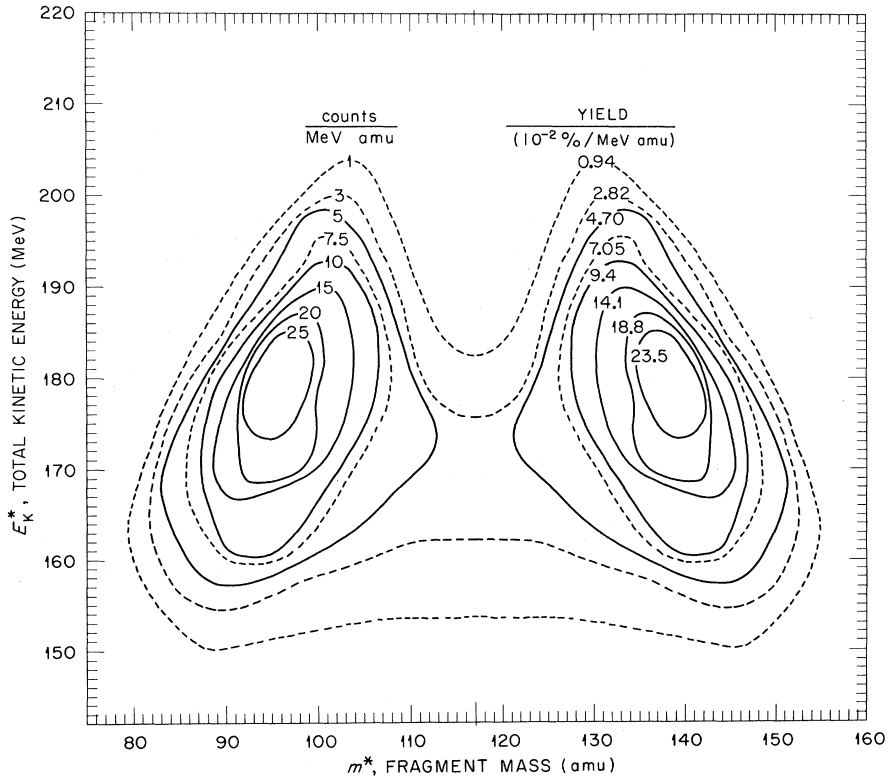

FIG. 2. Contour diagram of fission yields as a function of prompt fragment mass and total kinetic energy of both fragments for $^{233}U(p,f)$, $E_p = 8.5$ MeV.

with peaks occurring at heavy-fragment masses in the range 128–130 amu.

The peak-to-valley ratio of the mass distribution and other over-all features of the results for $^{238}U(p_{12},f)$ resemble those for $^{233}U(p_{8.5},f)$ more closely than those for $^{233}U(p_{13},f)$. This observation is perhaps correlated with the fact that ^{234}Np has a larger fissility parameter $[(Z^2/A)/(Z^2/A)_{crit}]$ than ^{239}Np.

B. Neutron Emission

In Fig. 7 contour diagrams show the total number of neutrons emitted, $\nu_T(m^*, E_K^*)$, as a function of pre-neutron-emission mass and total kinetic energy. In order to indicate the approximate boundaries of statistical significance, we have shown by a dashed line on each plot the contour corresponding to 3 to 5 events/MeV amu. General trends for all three systems are similar, exhibiting for all masses an increase in total neutron emission with decreasing total kinetic energy.

The average total number of neutrons emitted for all mass pairs is 5.6 for $^{233}U(p_{13},f)$, 5.0 for $^{233}U(p_{8.5},f)$, and 4.2 for $^{238}U(p_{12},f)$.

Figures 8 and 9 show the single-fragment neutron emission results $\nu(m^*)$ for $^{233}U(p_{13},f)$ and $^{238}U(p_{12},f)$, respectively. The quantity $\nu_T(m^*)$ is also given in these figures, and the prompt mass distributions $N(m^*)$ are replotted as light smooth curves for reference. The uncertainty in relative values of $\nu(m^*)$ over a small range of masses is small; an uncertainty assignment may, however, be made for an entire $\nu(m^*)$ curve whereby the curve may shift or rotate within error limits of ±0.5 neutron.

In Fig. 9 the function $\nu(m^*)$ determined by direct neutron counting[6] is also given; the data shown represent the sum of "prefission" and "postfission" neutrons from Ref. 6 and should be directly comparable with our $\nu(m^*)$ results. The agreement is satisfactory within experimental uncertainties.

Our $\nu(m^*)$ results for $^{233}U(p_{13},f)$ given in Fig. 8 have been compared with the results of Bishop *et al.* in Ref. 9. The agreement is within our experimental uncertainty of 0.5 neutron for all fragment masses except for fragments heavier than 140 amu in the heavy-mass wing of the distribution, where our results are systematically larger (up to one neutron). Bishop *et al.* do not give a complete analysis of their experimental uncertainties but state that their results are more accurate because of the inherently greater accuracy of a direct neutron counting method. If their errors were comparable with ours, the discrepancy could be accounted for. The possibility that we have underestimated our systematic errors,

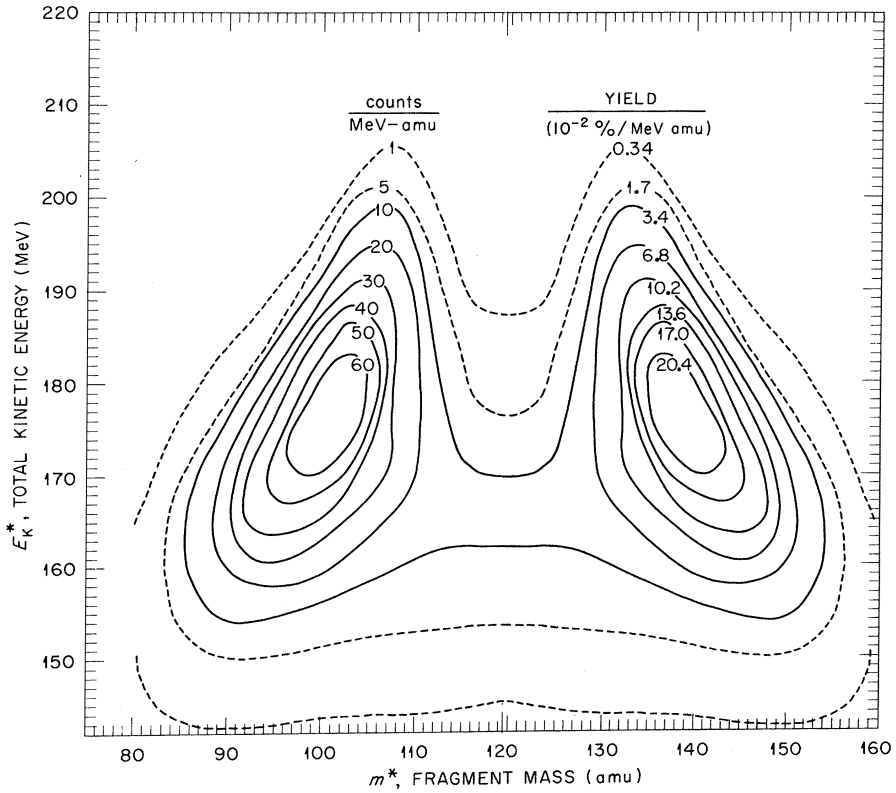

FIG. 3. Contour diagram of fission yields as a function of prompt fragment mass and total kinetic energy of both fragments for $^{238}U(p,f)$, $E_p = 12$ MeV.

particularly in the heavy-mass region cannot, however, be ruled out.

The primary $\nu(m^*)$ results for $^{233}U(p_{8.5},f)$ obtained in two separate sets of experiments are shown in Appendix I together with a discussion of the details of the experiments and the method of combining their results.

Final neutron-emission results for $^{233}U(p_{13},f)$ and $^{233}U(p_{8.5},f)$ are summarized in Fig. 10. In the lower portion of the figure, $\nu(m^*)$ is shown for both cases; the difference $\Delta\nu$ is plotted as a function of m^* in the upper portion. For reference, we have added light dashed curves in the lower portion of Fig. 10 showing $\nu(m^*)$ for thermal-neutron fission of ^{233}U as measured by Milton and Fraser[2] (long dashes) and by Apalin *et al.*[12] (short dashes). Although the mass of the compound nucleus is 234 amu for all the curves, direct comparison of the $^{233}U(p,f)$ and $^{233}U(n,f)$ data should be considered only with caution, since even-odd effects may significantly affect such a comparison.

The $\Delta\nu(m^*)$ results for ^{233}U at bombarding energies of 13 and 8.5 MeV can be compared with $\Delta\nu(m^*)$ results of Bishop *et al.*[9] at bombarding energies of 9.5 and 20 MeV. The results are qualitatively similar, except that Bishop *et al.* observe an upward trend of $\Delta\nu(m^*)$ beyond $m^* = 140$ amu, while no such trend is evident in Fig. 10.

Trends exhibited in the results for $^{233}U(p,f)$ and

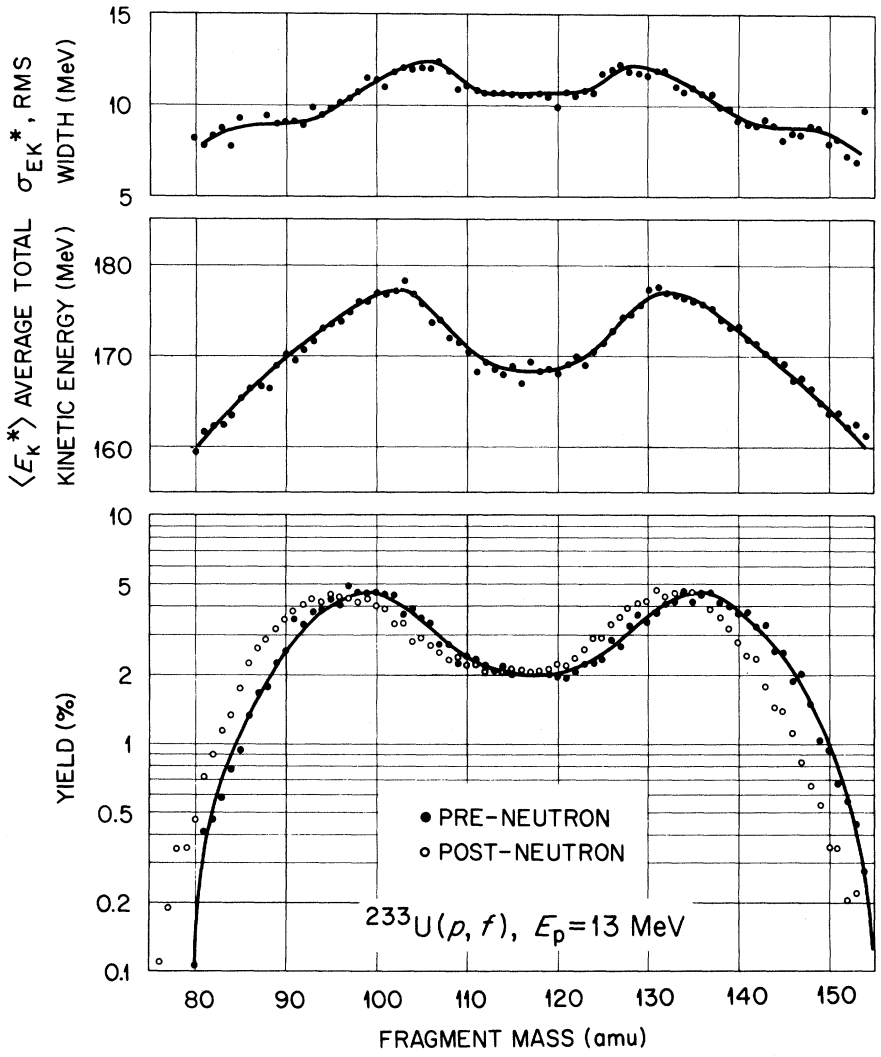

FIG. 4. Mass and energy results from $^{233}U(p,f)$, $E_p = 13$ MeV. Lower section: pre- and post-neutron-emission mass distributions. Center section: average total fragment kinetic energy, before neutron emission, as a function of prompt fragment mass. Upper section: root-mean-square width of the total kinetic energy distribution as a function of prompt fragment mass.

$^{238}U(p,f)$ discussed thus far are similar: a $\nu(m^*)$ curve generally increasing with increasing fragment mass, with a dip at $m^* \cong 132$, a $\nu_T(m^*)$ function showing relatively large values at symmetric and very asymmetric mass divisions, with somewhat lower values when the heavy fragments are near doubly magic ($Z \cong 50, N \cong 82$). Further discussion, in particular relating to the comparison of results at two compound-nucleus excitation energies, is contained in Sec. V.

In addition to the above results we have extracted information concerning the derivative $d\nu/dE_K^*$ as a function of mass. Statistical reliability of the $\nu(m^*, E_K^*)$ arrays for $^{233}U(p_{13},f)$ and $^{238}U(p_{12},f)$ was considered adequate for this purpose, and $d\nu/dE_K^*$ was obtained by a least-squares fit of $\nu(E_K^*)$ for each mass to a straight line. A plot of the slopes of these lines versus mass is given in Fig. 11.

IV. TOTAL ENERGY BALANCE

Analysis of the $^{233}U(p_{13},f)$ and $^{238}U(p_{12},f)$ data with respect to the total energy available for fission was carried out. The procedure followed here has been described previously.[5,13] An empirical value of the total energy released in fission E_T, was calculated for each mass from the sum of kinetic energies (measured) and fragment excitation energies (deduced from neutron results). These empirical values were compared with energy release estimates obtained from semiem-

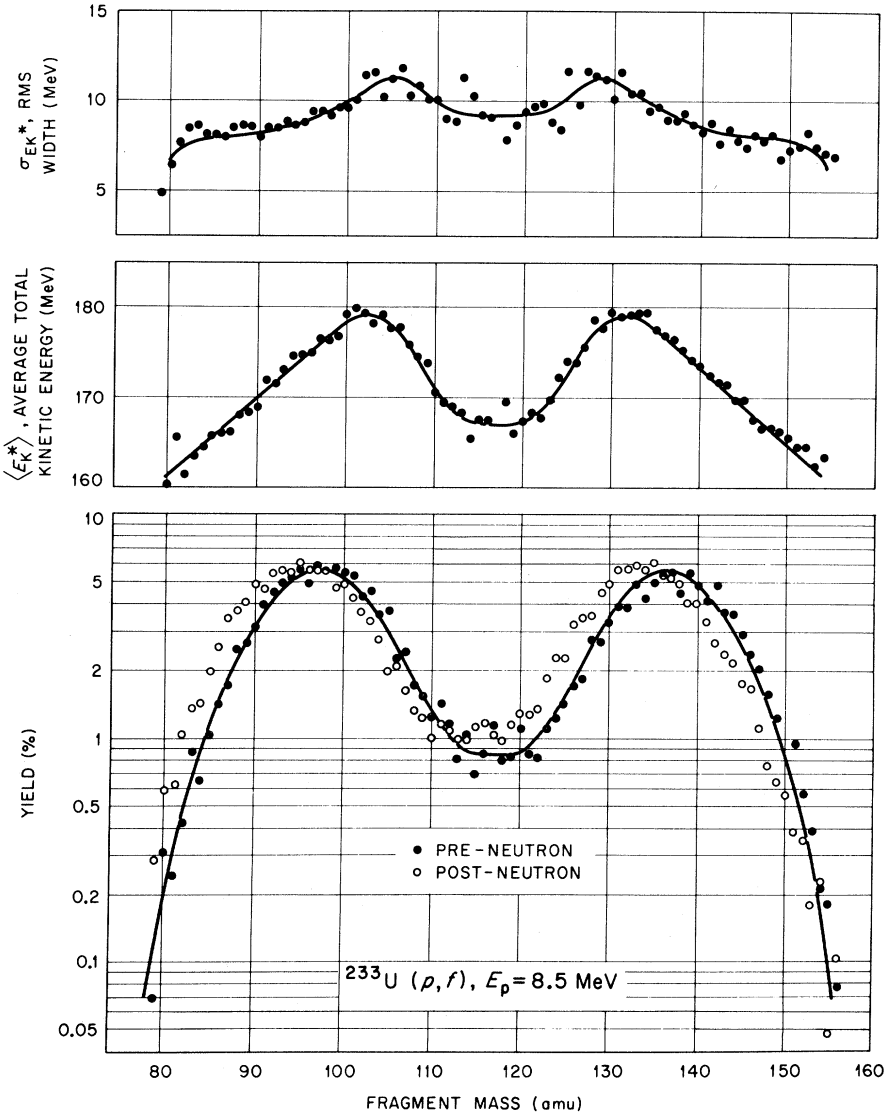

FIG. 5. Mass and energy results from $^{233}U(p,f)$, E_p=8.5 MeV. See Fig. 4 caption for other details.

pirical mass tables. The study was made with the mass formulas of Seeger.[14]

The excitation energy of a fragment was assumed to be equal to the sum of the binding and kinetic energies of the neutrons evaporated plus a term taking account of γ-ray emission. The binding energies were obtained from Seeger's masses,[14] where we have assumed the charge division to be that which is energetically preferred; the neutron kinetic energies were taken from estimates of Terrell,[15] and the number of neutrons $\nu(m^*)$ was taken from present results. The average prompt γ-decay energy was taken to be $\frac{1}{2}$ the neutron binding energy of the fragment after neutron emission.

The calculated values of E_T were obtained from the difference between the sum of the target and projectile masses and the sum of the fragment masses, plus the center-of-mass energy of the proton. For a given charge division, the curve obtained for E_T as a function of mass is approximately parabolic and has negative curvature.

The envelope of these curves may be compared with the empirical results as shown in Fig. 12. Two sets of parabolas appear in the ^{238}U(p_{12},f) case (the compound nucleus is ^{239}Np, with odd Z, even N), depending on whether one of the fragments is even-even or odd-odd. For the fission of the odd-odd nucleus ^{234}Np, the formation of an odd-odd fragment necessitates an even-even complementary fragment; the other possibility is the formation of an odd-even–even-odd fragment pair. The pairing energies are approximately equal for the two cases, thus the parabolas appear as only

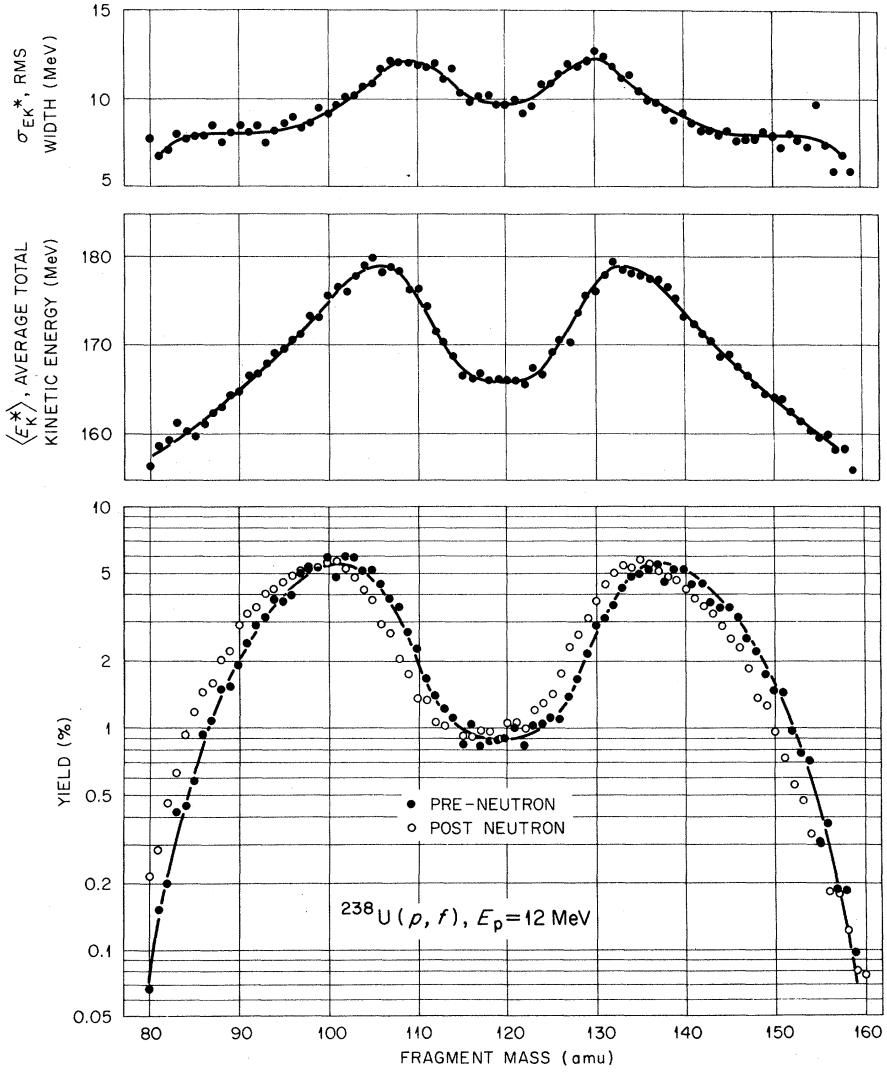

FIG. 6. Mass and energy results from ^{238}U(p,f), $E_p = 12$ MeV. See Fig. 4 caption for other details.

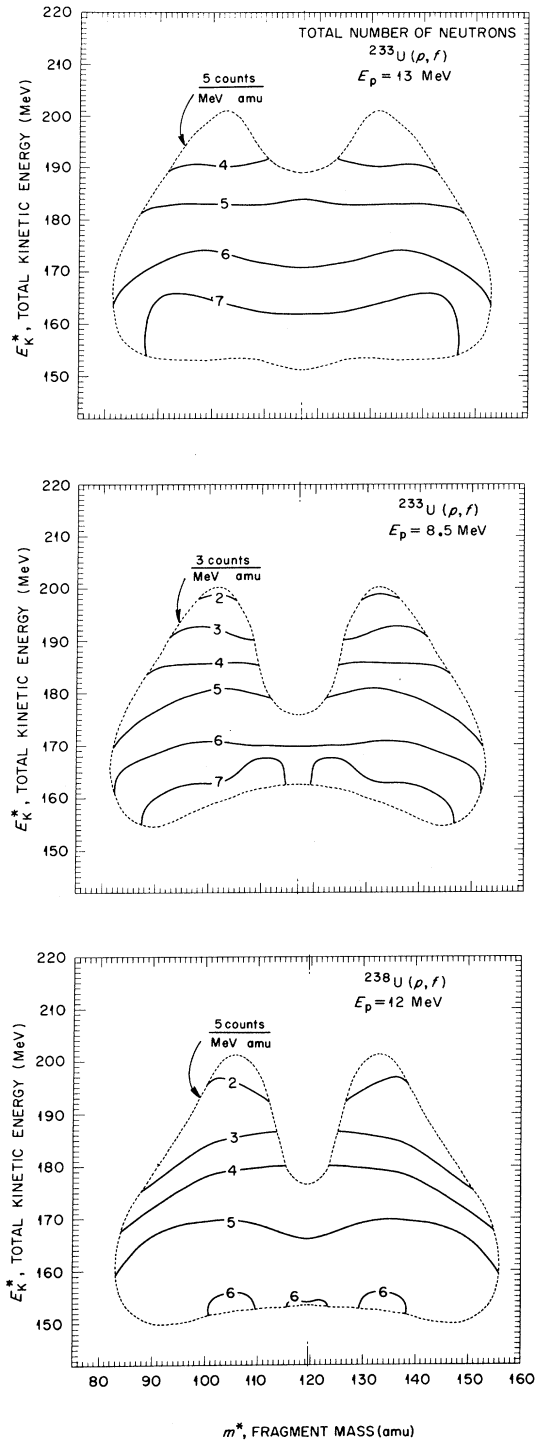

FIG. 7. Average total number of neutrons emitted from a fragment pair as a function of single fragment mass, m^*, and total fragment kinetic energy, E_K^*. Contours are shown for $^{233}U(p,f)$, E_p=13 MeV (upper section) and 8.5 MeV (middle section); and $^{238}U(p,f)$, E_p =12 MeV (lower section). A 3 or 5 counts/(MeV amu) contour is indicated by a dashed line for reference.

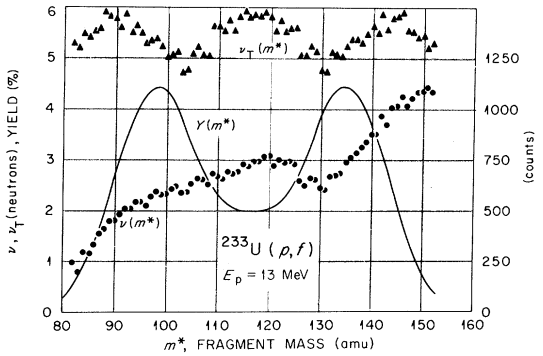

FIG. 8. Neutron results for $^{233}U(p,f)$, E_p=13 MeV. Average number of neutrons emitted per fragment (circles), and average total number of neutrons emitted from both fragments (triangles), as functions of fragment mass. The mass yield curve is shown for reference (smooth curve).

one set. In the ^{233}U case the difference between the mass-formula-deduced energy release and the empirical curve ranges from 5 MeV near symmetry to 10 MeV for large asymmetry. In the ^{238}U case the difference is also about 5 MeV near symmetry, but in the opposite direction, while away from symmetry the agreement is good. The shape of the empirical curve differs from the shape of the envelope of calculated curves in roughly the same way in both cases. Although the discrepancies in absolute values of E_T are somewhat larger than we might like, the uncertainties in the measurements (~1 neutron, or ~8 MeV in E_T), in the mass formulas, and in the conversion of neutron number to fragment excitation energy are sufficiently large so that the comparison of the calculated and empirical results is within present error limits.

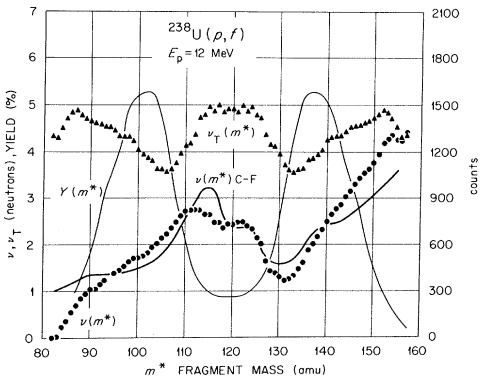

FIG. 9. Neutron results for $^{238}U(p,f)$, E_p=12 MeV. Results of the direct neutron counting experiment of Cheifetz and Fraenkel (Ref. 6) are shown as the solid curve. See caption to Fig. 8 for other details.

V. COMPARISON OF $^{233}U(p, f)$ AT PROTON ENERGIES OF 13 AND 8.5 MeV

It is indicated in Sec. I and Appendix II that the competition between fission and neutron evaporation is essentially the same for the two proton energies and that, therefore, any differences in the results for $^{233}U(p_{13}, f)$ and $^{233}U(p_{8.5}, f)$ may be attributed to the difference of 4.5 MeV in excitation energy of the ^{234}Np compound nucleus. The estimated excitation energies are 17.2 and 12.7 MeV, respectively.

Figure 13 shows, from bottom to top, the pre-neutron-emission mass-yield distributions, average total fragment kinetic energies as functions of fragment mass, and the rms widths of the total fragment kinetic energy distributions as functions of fragment mass for $^{233}U(p_{13}, f)$ and $^{233}U(p_{8.5}, f)$. The comparison of neutron yields is shown in Fig. 10. In the lower section of the figure, the number of emitted neutrons as a function of prompt fragment mass for $^{233}U(p_{13}, f)$ and $^{233}U(p_{8.5}, f)$ is represented by the heavy solid and dashed smooth curves, respectively. The difference in $\nu(m^*)$ between the 8.5- and 13-MeV cases $\Delta\nu$ is shown in the upper portion of Fig. 10. Throughout the light-fragment region ($m^* < 112$) there is little difference in $\nu(m^*)$ for 8.5- and 13-MeV proton-induced fission. The maximum difference occurs for $m^* \cong 130$, and the difference remains significant throughout the heavy-fragment group.

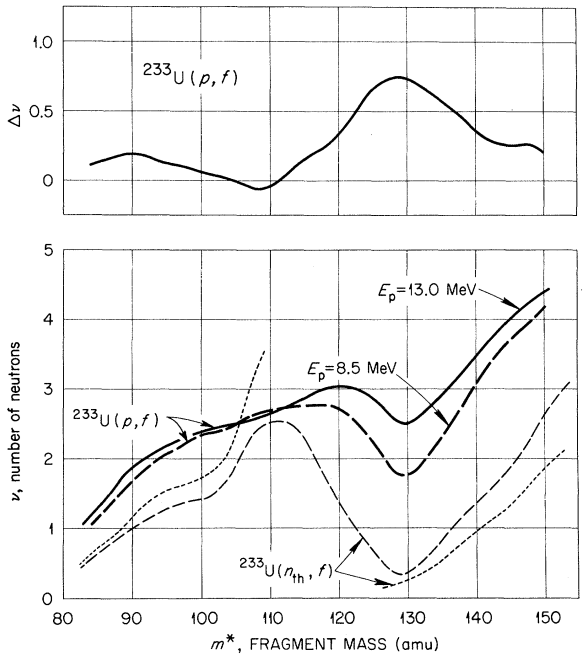

FIG. 10. Upper section: mass-by-mass differences in number of neutrons emitted, $\Delta\nu$, for $^{233}U(p, f)$ at E_p =13 MeV and at E_p =8.5 MeV. Lower section: comparison of fragment neutron yields $\nu(m)$ for $^{233}U(p, f)$, E_p =13 MeV (solid line), $^{233}U(p, f)$, E_p =8.5 MeV (heavy dashed line), and $^{233}U(n_{th}, f)$ (light long dashes Ref. 2, light short dashes Ref. 12). In the proton-induced fission the compound nucleus is ^{234}Np while in the neutron-induced fission the compound nucleus is ^{234}U.

In Fig. 14 the average total fragment excitation energy (calculated as described in Sec. IV), and average total fragment kinetic energy are plotted as functions of heavy-fragment mass m_H^* for each incident proton energy (center and lower portions). The difference ΔE_T in empirical E_T values for the two proton energies is also plotted as a function of m_H^* (upper portion). The horizontal line at 4.5 MeV in the upper part of Fig. 14 represents the expected value of ΔE_T based on the difference in the two laboratory bombarding energies (13- and 8.5-MeV). Center-of-mass effects are negligible (<0.02 MeV).

It can be seen that the increase (~6.7 MeV) in fragment excitation energy at $m^* = 130$ amu is greater than the increase in excitation energy of the compound nucleus, the excess excitation energy being compensated for by a decrease (~2.2 MeV) in total fragment kinetic energy. This situation also holds for other mass divisions in the region about $m_H^* = 130$.

For fragment masses $m^* \lesssim 96$ and $m^* \gtrsim 138$, the difference in total fragment kinetic energy for the two proton energies is small or zero, and for these mass divisions the extra compound-nucleus excitation energy simply gives rise to additional fragment excitation energy. From the data shown in Fig. 10, this additional excitation energy is accorded preferentially to the heavy fragment.

The trend indicated by these results is toward

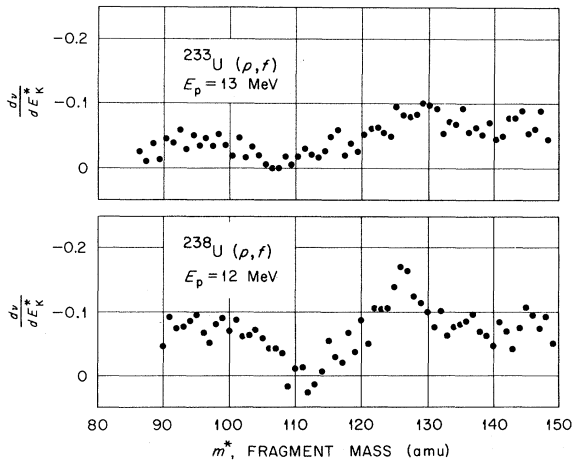

FIG. 11. Values of $d\nu/dE_K^*$ as derived from straight line fits to the $\nu(E_K^*)$ data for $^{233}U(p, f)$, E_p =13 MeV (upper section) and $^{238}U(p, f)$, E_p =12 MeV (lower section).

the washing out of the dip in the $\nu(m^*)$ curve in the heavy-fragment mass region near 130 amu, where closed-shell nuclei occur. If fragment shell effects are responsible for the sawtooth character of neutron-emission curves at low excitation energies[1] (e.g., thermal-neutron fission of ^{233}U, see Fig. 10), then our observations are consistent with the general assumption that shell effects tend to disappear with increasing excitation energy causing $\nu(m^*)$ to follow more nearly the linearly increasing function predicted by liquid-drop calculations.[16]

The measurements of the total kinetic energy, E_K^*, also tend to support this view. From the lowest section of Fig. 14 it can be seen that in the 13-MeV case the increase in E_K^* at symmetry and the decrease in E_K^* near fragment mass 130 (with respect to the 8.5-MeV data) establish a trend in the direction of liquid-drop predictions which, for this function, consist of parabolic curves peaked at symmetry.

The incremental changes in neutron emission and fragment kinetic energy may be qualitatively interpretated on the assumption of a static scission configuration [15, 17-20] as follows: Consider first the more asymmetric mass divisions, $m_L^* \lesssim 96$ and $m_H^* \gtrsim 138$ amu. No change in total fragment kinetic energy in this mass range indicates (most simply) no shape changes and therefore, no changes in fragment deformabilities with increasing compound-nucleus excitation energy. The incremental compound-nucleus excitation energy, then, simply gives rise to an equal increment in internal fragment excitation energy. If we assume that the temperature is uniform throughout the fissioning nucleus, then the internal excitation energy is expected to divide in the same ratio as the ratio of fragment masses. This is consistent with the larger increment in neutron emission observed in the heavy fragments.

Consider now the mass region in the neighborhood of $m_L^* \cong 104$ and $m_H^* \cong 130$ amu, where the maximum in $\Delta\nu$ occurs. The increment in compound-nucleus excitation energy $\Delta E_{CN}^* = 4.5$ MeV gives rise to increments in fragment excitation energy $\Delta E_{XL} \cong 0$ and $\Delta E_{XH} \cong 6.7$ MeV, obtained from observed values of $\Delta\nu_L$ and $\Delta\nu_H$, and to an observed increment in total fragment kinetic energy $\Delta E_K^* \cong -2.2$ MeV. Assuming no change in shape of the light fragment, we have calculated the change in shape of the heavy fragment that corre-

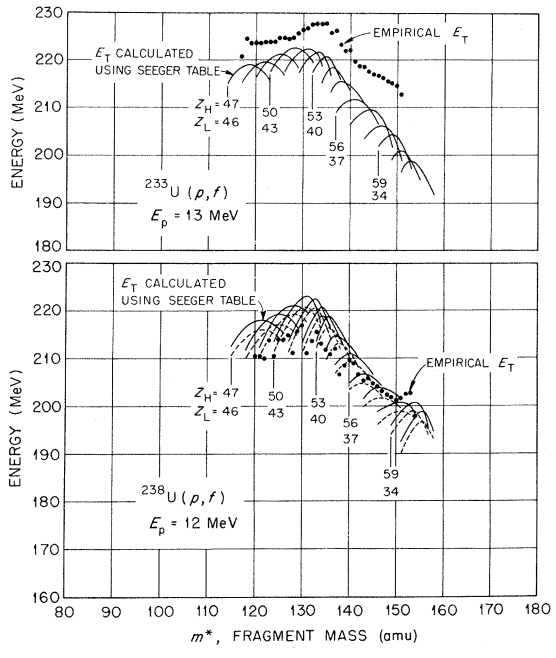

FIG. 12. Energy balance for ^{233}U(p,f), $E_p = 13$ MeV. (upper section) and ^{238}U(p,f), $E_p = 12$ MeV (lower section). Empirically calculated total energy (closed circles), and total energy as calculated from Seeger's mass formula (see Ref. 14) (parabolas) are shown. See text for discussion.

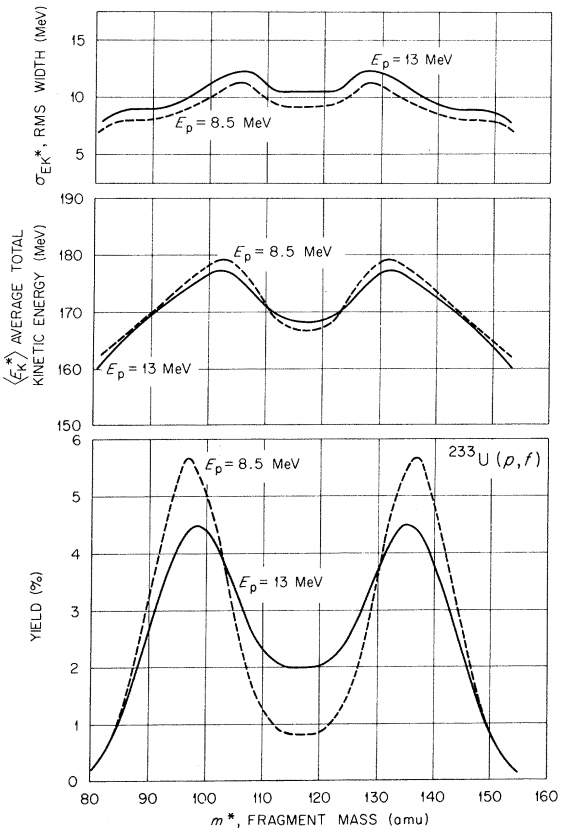

FIG. 13. Comparison of mass distributions, average total kinetic energy as a function of mass, and rms widths of the total kinetic energy distributions as a function of mass (bottom to top) for ^{233}U(p,f), $E_p = 13$ and 8.5 MeV.

sponds to a reduction $\Delta V_C \cong -2.2$ MeV in the mutual Coulomb repulsion potential energy, and have estimated[21] the corresponding increase in heavy-fragment deformation energy to be $\Delta V_{DH} \cong 2.8$ MeV ($\pm$~0.8 MeV).

A consistent picture of the division of the observed total increment in excitation energy can now be obtained as follows:

$$\Delta E_{XL} + \Delta E_{XH} = \Delta V_{DL} + \Delta V_{DH} + \Delta E_{IL} + \Delta E_{IH},$$

where ΔE_{IL} and ΔE_{IH} are the increments in the internal light- and heavy-fragment excitation energies, respectively. Substituting $\Delta V_{DL} = 0$, $\Delta V_{DH} = 2.8$ MeV, and $\Delta E_{XL} + \Delta E_{XH} = 6.7$ MeV, we obtain $\Delta E_{IL} + \Delta E_{IH} = 3.9$ MeV. If we divide the internal fragment excitation energy between the fragments in the same ratio as the fragment masses (for $m_L^* = 104$ and $m_H^* = 130$), we obtain $\Delta E_{IL} = 1.7$ MeV and $\Delta E_{IH} = 2.2$ MeV. This results in total fragment excitation energy increments

$$\Delta E_{XL} = \Delta V_{DL} + \Delta E_{IL} = 1.7 \text{ MeV},$$

$$\Delta E_{XH} = \Delta V_{DH} + \Delta E_{IH} = 5.0 \text{ MeV}.$$

These energies compare with $\Delta E_{XL} = 0$ and $\Delta E_{XH} = 6.7$ MeV obtained from observed values of $\Delta \nu_L$ and $\Delta \nu_H$. These values for ΔE_{XL} and for ΔE_{XH}, respectively, agree within the limits of experimental errors.

On the basis of the above discussion it would appear that the increase in E_{CN}^* has caused the heavy fragment to soften somewhat, thereby increasing its deformation energy ($\Delta V_{DH} \cong 2.8$ MeV) and correspondingly decreasing V_C (and therefore also E_K^*). It is intriguing that $\Delta V_{DH} + \Delta V_C \cong 0$, leaving ΔE_{CN}^* approximately equal to the increment in internal fragment excitation energy.

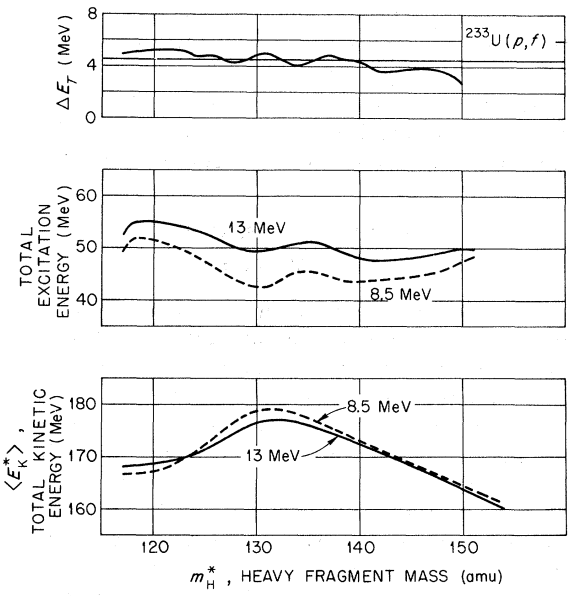

FIG. 14. Bottom to top: average total fragment kinetic energy, total fragment excitation energy, and the difference in the total energy available for fission, ΔE_T, as a function of heavy fragment mass for ^{233}U(p,f), E_p =13 and 8.5 MeV.

Upon consideration of the above points of discussion, we are tempted to suggest that a principle of conservation of shape-associated energies may be operative in this range of compound-nucleus excitation energies, whereby if an increase in E_{CN} causes one (or both) of the fragments to soften (i.e., increase deformability) the resulting increase in deformation energy V_D is compensated by a decrease in V_C with the increase in E_{CN}^* appearing as an equal increase in internal fragment excitation energy. That is, $\Delta V_{DL} + \Delta V_{DH} + \Delta V_C \cong 0$ and $\Delta E_{CN}^* = \Delta E_{IL} + \Delta E_{IH}$. Such a principle would be consistent with the present results over the entire fragment mass range.

Although this is a simple and apparently consistent interpretation of the data, it is clearly not unambiguous. An increased compound-nucleus excitation energy could lead to any of many possible combinations of increments in fragment deformation energies and internal excitation energies and still be consistent with the data. An additional source of ambiguity in interpretation occurs if the system has appreciable kinetic energy at scission.

We wish to thank G. F. Wells and the Oak Ridge tandem Van de Graaff staff for their support. The help of Frances Pleasonton with the early stages of these experiments is gratefully acknowledged. We also acknowledge helpful discussions with R. W. Lide, J. R. Nix, and P. A. Seeger.

APPENDIX I

In this Appendix we discuss the details of the various runs (experiments) listed in Table I as they relate to determination of the final results.

For the ^{238}U(p,f) experiment at $E_p = 12$ MeV, conditions were near optimum. The ^{252}Cf calibration experiment and ^{238}U(p,f) experiment were done under identical conditions, except for very small differences in source-to-detector distances. Thus a straightforward analysis yields the results given in the text.

Similarly, conditions were near optimum for the ^{233}U(p,f) experiment at $E_p = 13$ MeV labeled (d) in Table I. Here again the ^{252}Cf calibration experiment and the uranium experiment were done under identical conditions, except for very small differences in source-to-detector distances, and the data from this experiment were used for the ^{233}U(p_{13},f) results given in the text. For the purpose of this

Appendix, let us designate the $\nu(m^*)$ results of this experiment by $\nu^a_{13}(m^*)$.

To obtain a careful comparison of neutron emission results at two compound-nucleus excitation energies it is desired that the appropriate experiments be carried out under identical conditions at the two energies. This was done in the experiments labeled (a) and (b) in Table I, corresponding to proton energies 13 and 8.5 MeV, respectively.

Afterward, however, the target thickness was found to be ~190 μg/cm^2 instead of $\lesssim$60 μg/cm^2 as desired. Therefore the following procedure was followed: (1) In analysis of the three-parameter data of experiment (a), an empirical target-thickness correction was made by adding small increments to the raw data channel numbers. The magnitudes of the increments were varied within a small range until the resulting average single post-neutron-emission fragment masses, kinetic energies, and velocities agreed with those obtained in experiment (d) within 0.1%. The number of emitted neutrons, designated $\nu^a_{13}(m^*)$ for this discussion, was then calculated; these results are shown as closed circles in the lower portion of Fig. 15. (2) Without changing the analysis procedure in any way the data of experiment (b) were analyzed, yielding the results shown as open circles in the lower portion of Fig. 15 and here labeled $\nu^b_{8.5}(m^*)$. (3) The difference $\Delta\nu_{ab}(m^*) = \nu^a_{13}(m^*) - \nu^b_{8.5}(m^*)$ was calculated. (4) A complete analysis of the data was repeated, but without the empirical target-thickness correction.

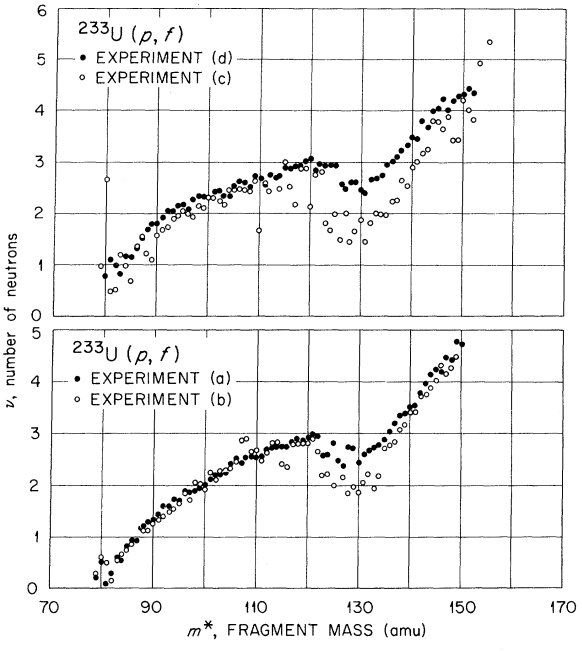

FIG. 15. Lower section: $\nu(m^*)$ results from experiment (a), ^{233}U(p_{13},f) closed circles, and experiment (b), ^{233}U$(p_{8.5},f)$, open circles. Upper section: $\nu(m^*)$ results from experiments (d), ^{233}U(p_{13},f), closed circles, and experiment (c), ^{233}U$(p_{8.5},f)$, open circles.

Although the absolute values of $\nu(m^*)$ were affected by the target-thickness correction, the $\Delta\nu_{ab}(m^*)$ results obtained in (4) above were essentially unchanged from those obtained in (3). Furhter, the absolute values of $\nu^a_{13}(m^*)$ obtained in (1) above agreed with those of $\nu^d_{13}(m^*)$ within 0.5 neutron uncertainty, although the $\nu^a_{13}(m^*)$ curve seems to be rotated counterclockwise just slightly with respect to $\nu^d_{13}(m^*)$.

An additional thin-target (~60 μg/cm^2) experiment, labeled (c) in Table I, was performed at $E_p = 8.5$ MeV. The detectors were the same as those of experiments (a) and (b), but were different from those of experiment (d). Also the number of events was limited to 8714, a number which is near the minimum required for reasonable statistical accuracy in an energy-energy-velocity experiment. Nonetheless, we have plotted the results $\nu^c_{8.5}(m^*)$ as open circles in the upper portion of Fig. 15 along with the $\nu^d_{13}(m^*)$ results, plotted as closed circles. It is seen that the agreement between $\nu^c_{8.5}(m^*)$ and $\nu^b_{8.5}(m^*)$ is within ~0.5 neutron. The difference $\Delta\nu_{cd}(m^*) = \nu^d_{13}(m^*) - \nu^c_{8.5}(m^*)$ was calculated.

Keeping in mind the possible uncertainties introduced by the use of different pairs of detectors, we have averaged $\Delta\nu_{cd}(m^*)$ and $\Delta\nu_{ab}(m^*)$ to obtain $\Delta\nu(m^*)$, our final curve for the difference between $\nu(m^*)$ for $E_p = 13$ MeV and $\nu(m^*)$ for $E_p = 8.5$ MeV; this result is shown in the upper portion of Fig. 10. The lower portion of Fig. 10 shows our $\nu(m^*)$ result for $E_p = 13$ MeV [experiment (d), as discussed above] and $\nu(m^*)$ for $E_p = 8.5$ MeV, obtained by subtracting $\Delta\nu(m^*)$ from $\nu(m^*)$ for $E_p = 13$ MeV.

APPENDIX II. EXPERIMENTAL UNCERTAINTIES

Error analysis for the energy-energy-time experimental method is complicated and estimates of the uncertainty in absolute number of neutrons emitted have been made on the basis of analyses in which various parameters were varied within the limits of their respective uncertainties. In general the uncertainty in ν is of the order of ± 0.5 neutron. This means that the $\nu(m^*)$ curves from these experiments may be too high or too low by 0.5 neutron, and also implies that the slope of the curve may be uncertain to the extent permitted by 0.5 neutron uncertainty in neutron yield at either end of the curve. In arriving at this estimate of the uncertainty in $\nu(m^*)$, an attempt was made to include possible systematic errors, e.g., those

that may occur from uncertainties in the calibration of detectors and timing apparatus, and also to include errors that may arise from the averaging processes inherent in the method and from statistical fluctuations in the data. An estimate of the statistical error in $\nu(m^*)$ was obtained by calculating the deviation of the neutron yield points from a smooth curve drawn through averaged data points. The rms deviation of the points from the smooth curve was 0.077 neutron for the $^{233}U(p_{13},f)$ experiment involving 51 193 events, and 0.166 neutron for the $^{233}U(p_{8.5},f)$ experiment involving 8714 events. In carefully performed experiments, run under identical conditions and designed for direct comparison, the relative uncertainty in $\nu(m^*)$ may be reduced to ~0.2 neutron.

The competition between deexcitation by fission and by neutron evaporation was considered for the fissioning systems studied here. In the 13-MeV proton-induced fission of ^{233}U, the compound nucleus ^{234}Np is formed with a calculated excitation energy of ~17.2 MeV.[22] Since the fission barrier of ^{234}Np is estimated to be ~6.0 MeV[23] and the neutron binding energy ~6.1 MeV,[22] there is a possibility of fission occurring after the evaporation of a neutron.

Huizenga and Vandenbosch[24] have compiled information from photofission and spallation experiments regarding Γ_n/Γ_f, the ratio of neutron width to fission width, as a function of compound-nucleus mass number and excitation energy. From this compilation Γ_n/Γ_f for $^{233}U+p$ is found to be ~0.22, and thus the contribution from second-chance fission is about 18%. There appears to be no strong dependence of Γ_n/Γ_f on compound-nucleus excitation energy in the uranium mass region.

In the 12-MeV proton-induced fission of ^{238}U, the compound nucleus ^{239}Np is formed with a calculated excitation energy of ~17.3 MeV.[22] The fission barrier of ^{239}Np is estimated to be ~5.6 MeV[23] and the neutron binding energy ~6.2 MeV.[22] Huizenga and Vandenbosch[24] indicate that Γ_n/Γ_f is ~1.0. Therefore, in about one-half of the fission events a neutron is evaporated from the compound nucleus before fission occurs; that is, about one-half of the observed events are from the fission of ^{239}Np at ~17.3-MeV excitation energy and one-half from the fission of ^{238}Np at ~11.1-MeV excitation. The work of Chiefetz and Fraenkel[6] also indicates that Γ_n/Γ_f is ~1.0 for this case.

In the present work, the analysis of the $^{238}U(p,f)$ data has been carried out as though the mass number of the fissioning nucleus were equal to 239 amu. Thus on the average an additional 0.5 neutron, or 0.25 neutron per fragment, is included in the present results over the entire fragment mass range. Correction for this effect can be made, but has not been included here since this error (0.25 neutron per fragment) is within the over-all uncertainty of the results (±0.5 neutron per fragment).

Simple estimates have been made concerning possible effects of angular momentum on the comparison of the 8.5- and 13-MeV experiments. These estimates have shown that the maximum rotational energy, E_R, of the compound nuclei under study, is small (<0.1 MeV). The difference in E_R for the 13- and 8.5-MeV cases is, therefore, insignificant.

The largest contribution to dispersion in the determination of fragment mass from time-of-flight measurements is due to neutron emission from the fragments. Dispersive effects are particularly important for the low-excitation and spontaneous fission of heavy nuclei, where large slopes are present in certain regions of the mass distributions. Calculations for the medium-excitation fission cases studied in this paper, however, have shown the effects of dispersion to be small[25] and the data presented here have not been corrected for dispersion due to neutron emission.

The target and backing material in experiments of this kind should be as thin as possible. The backing degrades the energy of a fragment passing through it while the target deposit both degrades and disperses the energies of the fission fragments. Target-thickness effects have been discussed in Appendix I.

In an accurate energy-energy time experiment, for each fission fragment incident on the detector remote from the target, the complementary fragment should be incident on the detector near the target. Thus the effect of a finite source, the effect of the motion of the compound nucleus, and the noncolinearity of the fragments in the center-of-mass system caused by fragment neutron-emission must be taken into account. The first two effects are readily calculated. As to the third, Lide[26] has studied the effects of prompt neutron emission on the direction and time of flight of fission fragments. From his calculations, the geometry required to detect complementary fragments may be estimated. The target and detector geometry chosen for the present work was such that for all fragments incident on the remote detector, more than 98% of the complementary fragments were detected by the near detector.

The effect of pulse pileup was also considered as a source of error and dispersion in the present measurements. For a proton beam current of 100 nA, approximately 20 000 protons per sec were scattered into the near detector, and, on the average, these protons deposited ~1.5 MeV of

energy in the detector. From these measurements, it was estimated that pileup of a proton pulse on a fission fragment pulse occurred for approximately 4% of the fragment pulses detected. To avoid excessive pileup, proton beam currents in the experiments were limited to approximately 100 nA. The energies of fragments detected in the near detector were then, on the average, incorrect by only 0.06 MeV, causing essentially no error in the results.

---

†Research sponsored by the U. S. Atomic Energy Commission under contract with the Union Carbide Corporation. This work is based on part of a dissertation submitted by S. C. Burnett to the faculty of the University of Tennessee, Knoxville, Tennessee, in partial fulfillment of the requirements for a Ph.D. degree in Physics.

*Present address: Los Alamos Scientific Laboratory, Los Alamos, New Mexico.

[1]J. Terrell, Phys. Rev. 127, 880 (1962), and references therein.

[2]J. C. D. Milton and J. S. Fraser, in *Proceedings of the Symposium on the Physics and Chemistry of Fission, Salzburg, 1965* (International Atomic Energy Agency, Vienna, Austria, 1965), Vol. II, p. 39.

[3]E. E. Maslin, A. L. Rodgers, and W. G. F. Core, Phys. Rev. 164, 1520 (1967).

[4]M. Derengowski and E. Melkonian, Phys. Rev. C 2, 1554 (1970).

[5]E. Konecny and H. W. Schmitt, Phys. Rev. 172, 1213 (1968).

[6]E. Cheifetz and Z. Fraenkel, Phys. Rev. Letters 21, 36 (1968).

[7]F. Plasil, R. L. Ferguson, and H. W. Schmitt, in *Proceedings of the Second Symposium on the Physics and Chemistry of Fission, Vienna, 1969* (International Atomic Energy Agency, Vienna, Austria, 1969), p. 505.

[8]S. C. Burnett, R. L. Ferguson, F. Plasil, and H. W. Schmitt, Phys. Rev. Letters 21, 1350 (1968).

[9]C. J. Bishop, R. Vandenbosch, R. Aley, R. W. Shaw, Jr., and I. Halpern, Nucl. Phys. A150, 129 (1970).

[10]H. W. Schmitt, R. W. Lide, and F. Pleasonton, Nucl. Instr. Methods 63, 237 (1968).

[11]It is convenient to distinguish between the variables associated with excited prompt pre-neutron-emission fragments and those associated with post-neutron-emission fragments by labeling the former with an asterisk.

[12]V. F. Apalin, Yu. N. Gritsyuk, I. E. Kutikov, V. I. Lebedev, and L. A. Mikaelian, Nucl. Phys. 71, 553 (1965).

[13]H. W. Schmitt, J. H. Neiler, and F. J. Walter, Phys. Rev. 141, 1146 (1966).

[14]P. A. Seeger, in *Proceedings of the Third International Conference on Atomic Masses, 1967* (University of Manitoba Press, Winnipeg, Canada, 1967), p. 85; P. A. Seeger and R. C. Perisha, Los Alamos Scientific Laboratory Report No. LA-3751, 1967 (unpublished).

[15]J. Terrell, in *Proceedings of the Symposium on the Physics and Chemistry of Fission, Salzburg, 1965* (International Atomic Energy Agency, Vienna, Austria, 1965), Vol. II, p. 3.

[16]J. R. Nix and W. J. Swiatecki, Nucl. Phys. 71, 1 (1965).

[17]J. C. D. Milton and J. S. Fraser, Can. J. Phys. 40, 1626 (1962).

[18]R. Vandenbosch, Nucl. Phys. 46, 129 (1963).

[19]J. M. Ferguson and P. A. Read, Phys. Rev. 139, B56 (1965).

[20]H. W. Schmitt, in *Proceedings of the Second Symposium on the Physics and Chemistry of Fission, Vienna, 1969* (International Atomic Energy Agency, Vienna, Austria, 1969), p. 67.

[21]The increase in heavy-fragment deformation energy was estimated as follows: The fragments were considered to be two touching prolate spheroids. The shape of the light fragment was considered to remain unchanged. The change in eccentricity of the heavy fragment required to produce the observed ΔE_K^* was calculated. Using Seeger's relationship (see Ref. 14) between energy and nuclear deformation, including shell effects, the change in fragment deformation energy was obtained from the calculated shape change. The uncertainty in the calculation is due to the uncertainty in the absolute value of the spheroid eccentricity and to the approximations of Seeger's method. The region of deformation in which the change in deformation was evaluated was largely arbitrary.

[22]J. H. E. Mattauch, W. Thiele, and A. H. Wapstra, Nucl. Phys. 67, 1 (1965).

[23]V. E. Viola, Jr., and B. D. Wilkins, Nucl. Phys. 82, 65 (1966).

[24]J. R. Huizenga and R. Vandenbosch, in *Nuclear Reactions*, edited by P. M. Endt and P. B. Smith (North-Holland Publishing Company, Amsterdam, The Netherlands, 1962), Vol. II, p. 42.

[25]S. C. Burnett, Oak Ridge National Laboratory Report No. ORNL-TM-2272, 1968 (unpublished).

[26]R. W. Lide, Oak Ridge National Laboratory Report No. ORNL-3338, 1962 (unpublished).